Preprint Title Four self-made free surface electrospinning devices for high-throughput preparation of quality nanofibers

Authors Yue Fang and Lan Xu

Article Type Full Research Paper

ORCID® iDs Yue Fang - https://orcid.org/0000-0002-8825-4966; Lan Xu - https://orcid.org/0000-0003-2185-4104

Four self-made free surface electrospinning devices for high-throughput preparation of quality nanofibers

*Yue Fang, Lan Xu**
National Engineering Laboratory for Modern Silk, College of Textile and Engineering, Soochow University, 199 Ren-ai Road, Suzhou 215123, China
Correspondence: yfang5279@stu.suda.edu.cn (Y.F.); lanxu@suda.edu.cn (L.X.); Tel.: +86-512-65884521 (L.X.)

Abstract

Four different self-made free surface electrospinning (FSE) devices, namely, modified bubble-electorspinning (MBE) device, modified free surface electorspinning (MFSE) device, oblique section free surface electorspinning (OSFSE) device and spherical section free surface electrospinning (SSFSE) device, were presented to obtain high-throughput preparation of high quality nanofibers in this paper. The preparation mechanisms of these four FSE device were studied by simulating the electric field distribution using Maxwell 3D, due to the importance of electric field in the FSE process. And the effects of them on the morphology and yield of nanofibers were investigated by experiments. The experimental data agreed with the simulation results of electric field, and showed these four FSE device all could be used to prepare high quality nanofibers in large quantities. Meanwhile, comparing the spinning effects of these four FSE device, the results illustrated the SSFSE device was the optimal FSE device because of the highest quality and yield of nanofibers, and its yield could reach 20.03 g/h at the applied voltage of 40 kV.

Keywords: free surface electrospinning device; electric field; high-throughput preparation; nanofibers; mechanism; Maxwell 3D

1. Introduction

Due to their excellent properties, such as high surface-to-volume ratios and high porosities, nanomaterials have become more and more important in industrial manufacturing. As one of the most important methods for preparing nanomaterials, electrospinning (ES) [1-3] has been receiving much attention [4-7]. But with the advancement of nanotechnology and the increasing performance requirements of nanomaterials, the fatal shortcoming of the traditional ES process, low yield [8, 9], has received more attention. Many attempts have focused on improving the production of the ES technique. Ding et al. [10] has electrospun nanofibers using a multiple-jet ES system. Krishnamoorthy et al. [11] demonstrated an ES setup consisting of 24 (8×3) nozzles for the large-scale production of aligned ceramic nanofibers. And Kim et al. [12] developed an upward high-speed cylinder-type ES system with 120 needles in each cylinder to obtain the mass production of nanofibers.

In spite of the high production, there still remain some problems during these ES processes, such as the blocked needles and the interactions between jets.

Accordingly, many needleless electrospinning methods were presented to obtain high-throughput production of nanofibers in recent years [13-23]. Niu et al. [13] prepared high-throughput polyacrylonitrile (PAN) nanofibers using a needleless electrospinning method. He et al. [14, 15] presented a bubble-electrospinning (BE) device as an effective method for preparing nanofibers in batches. Thoppey et al. [16] successfully prepared Poly(ethylene oxide) (PEO) nanofibers using a modified ES device with a bowl collector. Jiang et al. [17] obtained mass preparation of PAN nanofibers by a free surface ES device. Wu et al. [18] studied the high throughput tip-less electrospinning via a circular cylindrical electrode. Shin et al. [19] used a multiple vertical rod setup for needless ES device to fabricate submicron polymer fibers. And Moon et al. developed a syringeless electrospinning technique with a helically probed rotating cylinder for preparing a nanofiber web [20]. The spinning parameters and yields of the established ES techniques were illustrated in a comparative table (see Table 1).

Table 1. The spinning parameters and yields of the established ES techniques

ES method	Fiber material	Spinning voltage	Yield
Single needle ES [8, 9]	Polyvinylpyrrolidone (PVP)	15-60 kV	0.01-0.1 g/h
Multi-nozzle ES [11]	PVP	15 kV	Several times of single needle ES
Coil ES [13]	Polyacrylonitrile (PAN)	60 kV	23g/h
BE [15]	Polyvinyl alcohol (PVA)	35 kV	3g/h
Bowl ES [16]	Poly(ethylene oxide) (PEO)	55kV	0.684 g/h
Free surface ES [17]	PAN	70kV	100 times of single needle ES
Tip-less ES [18]	PEO	68kV	260 times of single needle ES
Needleless vertical rods ES [19]	PVA	50kV	1.92 g/h
ES with a helically probed cylinder [20]	PAN	17kV	3.2g/h
MBE [21]	PVA	30-70 kV	19.8-72 g/h
MBE[23]	Silk fibroin (SF)	50kV	3.1 g/h

In our previous work [21, 22], a modified bubble-electrospinning (MBE) method was proposed to fabricate high quality PAN nanofibers with high yields. And the mass production of silk fibroin nanofibers was obtained successfully by this method [23]. The schematic presentation of the MBE device was illustrated in Fig.1 (A).

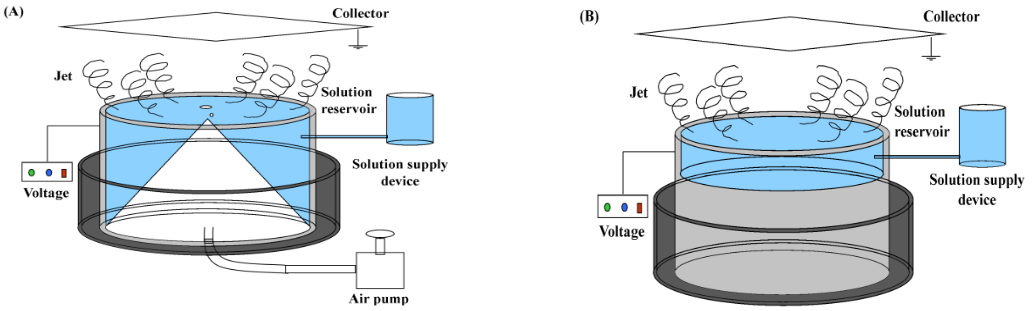

Figure 1. The schematic presentation of MBE [21] and FSE devices without an air pump.

As shown in Fig.1 (A), the MBE device mainly consisted of a solution reservoir, a variable high-voltage power generator, an air pump, a collector, and a solution supply device. Moreover, the solution reservoir was the main spinning part of MBE device, which included a copper pipe and a cone-shaped polymer nozzle. Based on the MBE device, three other self-made free surface electorspinning (FSE) devices, namely, modified free surface electorspinning (MFSE) device, oblique section free surface electorspinning (OSFSE) device and spherical section free surface electrospinning (SSFSE) device, were presented to obtain high-throughput preparation of high quality nanofibers through the modifications of solution reservoirs in this paper. Compared to the MBE, three other FSEs devices without an air pump, as illustrated in Fig.1 (B), only applied electric field forces to form jets on the surface of the spinning solution by overcoming its surface tension.

The effects of four FSE devices, which were MBE, MFSE, OSFSE and SSFSE device, on the morphology and yield of nanofibers were investigated experimentally and compared. Then the differences between them were explained by simulating the distribution of the electric field using Maxwell 3D. The results showed these four FSE devices all could be used to prepare high quality nanofibers in large quantities, and the SSFSE device was the optimal FSE device because of the highest quality and yield of nanofibers.

2. Experimental details

2.1 Materials

Polyacrylonitrile (PAN, MW = 15w) was provided from Beijing Lark Branch Co., Ltd. (Beijing, China). Sodium dodecyl benzene sulfonate (SDBS) was purchased from Sinopharm Chemical Reagent Co., Ltd. (Shanghai, China). N,N-dimethylformamide (DMF) was supplied from Shanghai Chemical Reagent Co. Ltd. (Shanghai, China). The spinning solution was obtained by dissolving 10 wt % of PAN and 1 wt% of SDBS in DMF under magnetic stirring at 60°C for 4h to get transparent liquid using a thermostatic magnetic stirrer (DF-101S, Xinrui Instrument Factory, Changzhou, China).

2.2 Apparatus

Four kinds of FSE apparatuses with different solution reservoirs, which were modified bubble-electorspinning (MBE) device, modified free surface electorspinning (MFSE) device, oblique section free surface electorspinning (OSFSE) device, and spherical section free surface electrospinning (SSFSE) device, were designed and made by ourself. Based on the MBE apparatus [14], as illustrated in Fig.1(B), three other apparatuses all consisted of a self-made copper solution reservoir, a grounded collector over the reservoir, and a variable high-voltage power generator (0-150 kV, TRC2020, Dalian Teslaman Technology Co., LTD), whose the positive terminal was directly connected to the solution reservoir. The schematic diagrams of these four solution reservoirs with different structures were illustrated in Fig.2.

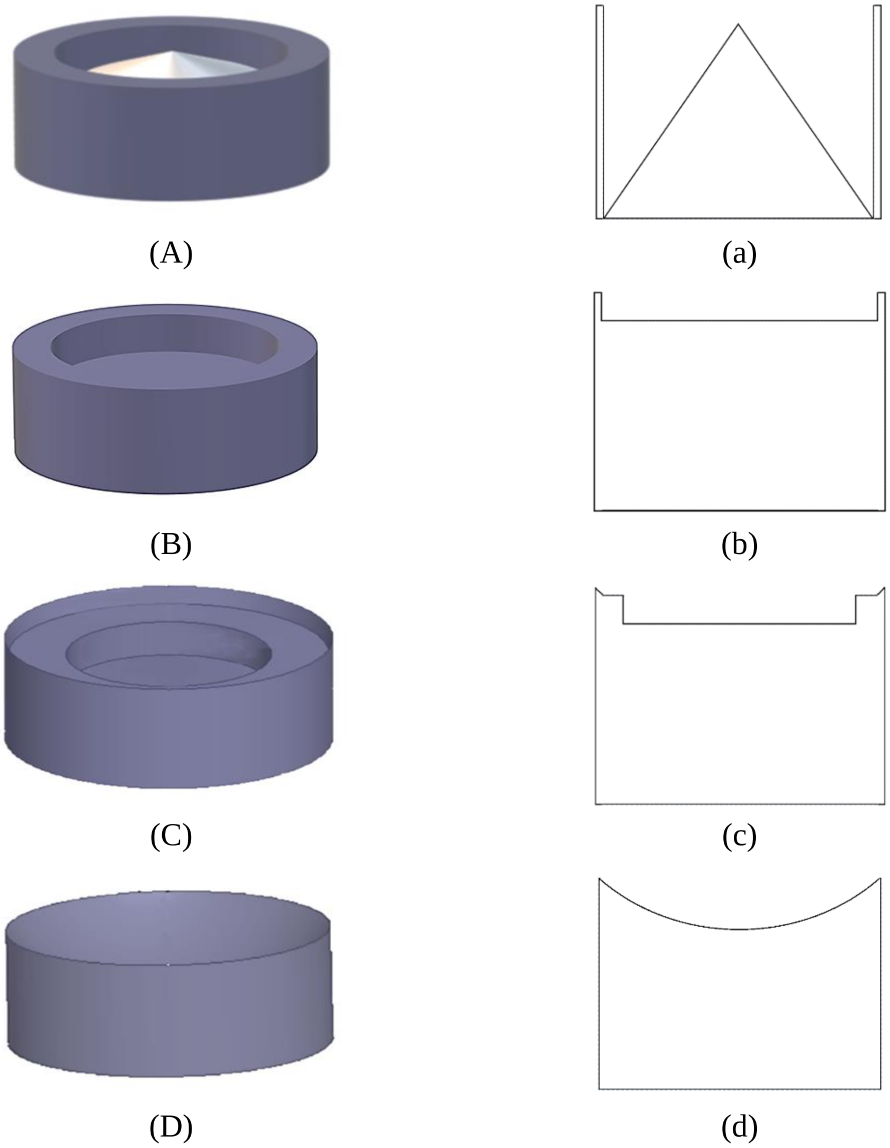
(A) (a)
(B) (b)
(C) (c)
(D) (d)

Figure 2. The schematic diagrams of the four solution reservoirs.

As shown in Fig.2, (A), (B), (C) and (D) were the 3D schematic diagrams of MBE, MFSE, OSFSE and SSFSE device respectively, moreover, (a), (b), (c) and (d) were their corresponding longitudinal cross-sectional views. The solution reservoir of MBE was a copper cylinder with a height of 30 mm, an outer diameter of 40 mm and a wall thickness of 2 mm, which contained a nylon cone shaped air nozzle with a height of 28mm and a bottom diameter of 36mm. The solution reservoir of MFSE device was a copper cylinder with a height of 30 mm and an outer diameter of 40 mm, in which a cylindrical groove with a radius of 18 mm and a height of 5 mm was dug from its upper surface. The solution reservoir of OSFSE device was similar to that of MFSE device, but in which the groove was made up of a circular truncated cone with a height of 2 mm, a upper bottom diameter of 40 mm and a lower bottom diameter of 36 mm, as well as a cylinder with a height of 8 mm and a diameter of 32mm, as exhibited in Fig.2(c). The solution reservoir of SSFSE device was a copper cylinder with a height of 30 mm and an outer diameter of 40 mm, which was truncated by a ball with a radius of 50mm.

2.3 Self-made FSE devices

According to our previous works [21-23], the spinning parameters of these four self-made FSEs devices were set as follows: the applied voltages were 40kV, and the working distances from the solution reservoir to the grounded collector were 18cm, and the collector surfaces (200 mm × 200 mm) were covered with conductive aluminum foil in order to easily remove the electrospun nanofiber membranes for further measurements. All the FSE experiments were carried out at room temperature (20℃) and at a relative humidity of 60%.

The spinning processes of different solution reservoirs were recorded using a high-speed camera at a frame rate of 100 frames/s (VRI-Phantom-VEO-L, Ametek, California, USA), as shown in Fig.3, Fig.4 and Fig.5. It could be seen the multiple jets generated in the MBE process were concentrated primarily near the top edge of the copper reservoir and the top of the bubble. The multiple jets produced in the MFSE process were mainly concentrated near the top edge of the reservoir, while the multiple jets generated in the OSFSE and SSFSE processes appeared on the entire solution surface. Comparing these photographs of the FSE processes, it was obvious that the number of jets produced in the MBE process was minimal, and the numbers of jets generated in the OSFSE and SSFSE processes were maximal relatively.

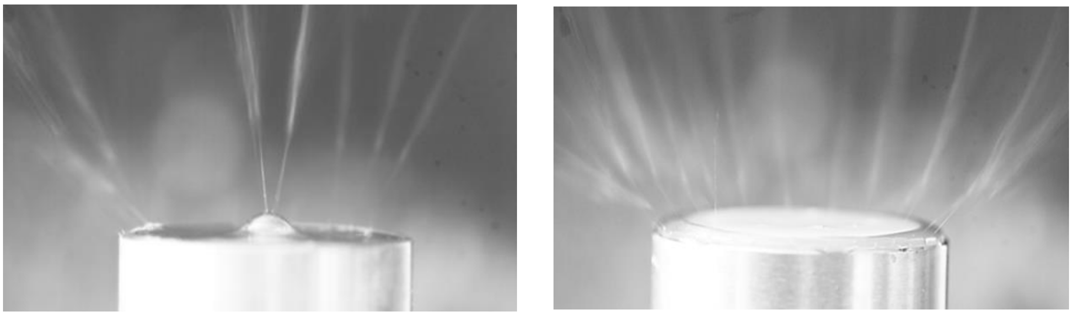

(a) MBE process (b) MFSE process

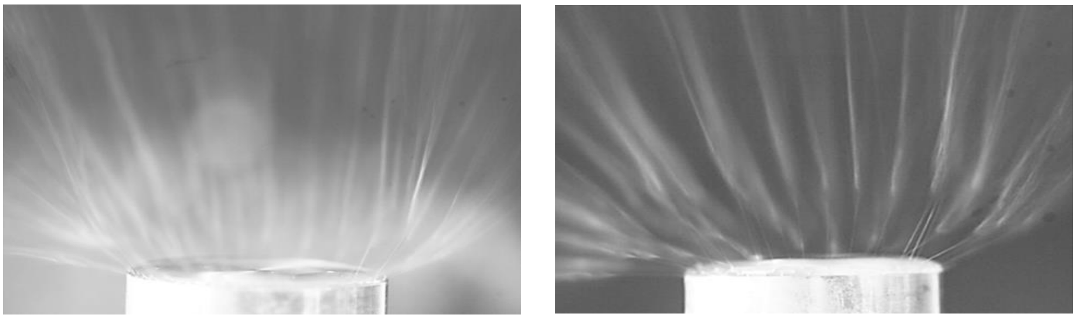

(c) OSFSE process (d) SSFSE process

Figure 3. Photographs of the MBE, MFSE, OSFSE, and SSFSE processes.

The jet initiation process occurring in the OSFSE process was observed from a side view perspective by the high-speed camera, as shown in Fig. 4. It could be found that after an electronic field was applied on the solution surface, in which the applied voltage (40 kV) was over the threshold voltage, a deformation of the fluid at the top edge of the solution reservoir was observed immediately in the first two seconds. And a Taylor cone-like protrusion produced a jet formation after 2 s. As time went on, the fluid deformations generated at the initiating period developed rapidly from the reservoir top edge to the center, while more and more Taylor cone-like protrusions were formed and resulted in more jets on the entire solution surface. After 15 s, the OSFSE process was allowed to stabilize.

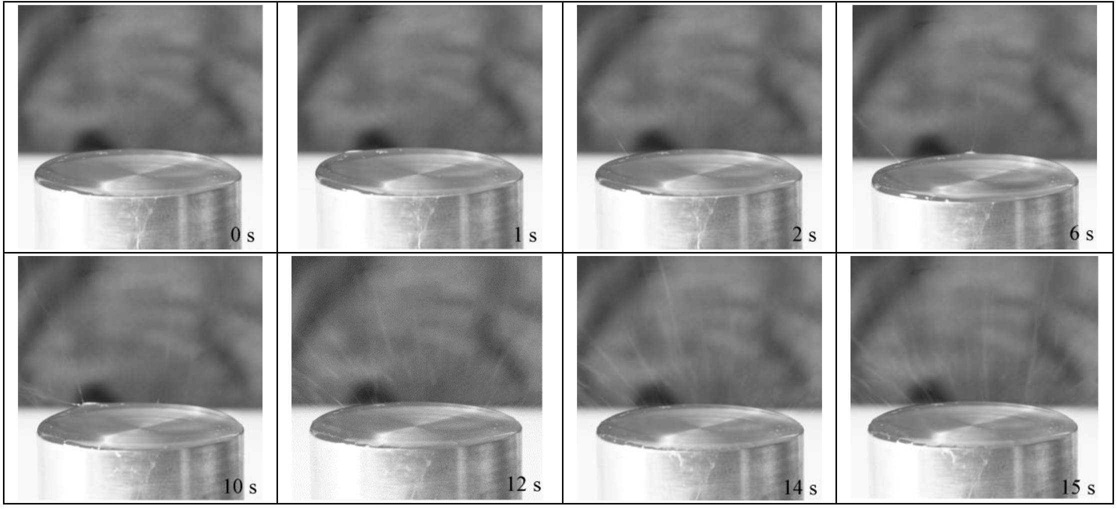

Figure 4. Sequential pictures of the jet initiation process occurring in the OSFSE process. The voltage was turned on and remained at the amplitude (40 kV) throughout the spinning process.

Fig.5 illustrated the sequential camcorder pictures of the jet formation process in the OSFSE process, which were obtained from a side view perspective of the high-speed camera. At the initiating period (10-80 ms), the fluid at the top edge of the solution reservoir was pulled upward by an applied electric field force. Then the fluid elongated, sharpened and became a Taylor cone-like protrusion during 80-110 ms. Finally, the fluid deformation resulted in a jet formation at 120 ms.

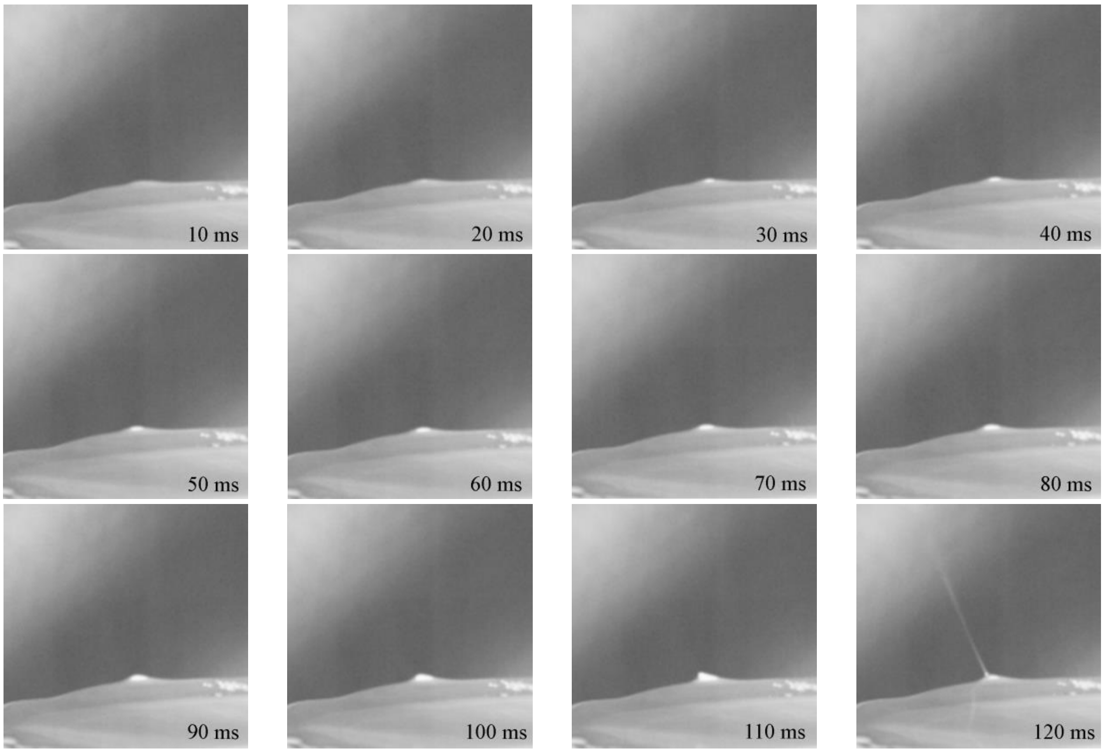

Figure 5. Sequential pictures of the jet initiation process in the OSFSE process. The voltage was turned on and remained at the amplitude (40 kV) throughout the spinning process.

It could be seen from Figs. 4 and 5 that the working principle of free surface electrospinning was to overcome the surface tension of the spinning solution using the electric field force generated by the applied electric field, then form jets on the solution surface, finally make the jets move to the collector and be stretched into nanofibers. Fig.6 showed the forces experienced on one of the jets produced in a FSE process when an electric field was applied between the solution reservoir and the collector, in which the airflow resistance and environmental interference were excluded. According to Fig. 6, the horizontal component the of viscous force F_1 produced a centripetal force resulting in the shrinking of the radius of whipping circle, and the vertical resultant force F_2 provided the kinetic energy of the jet, impelled the movement of the jet to the copper mesh collector, as well as supplied the stretching of the jet, which could be calculated respectively as follows:

$$F_1 = \tau \sin\alpha = (av + bv^2)\sin\alpha \tag{1}$$

$$F_2 = F_E - \tau\cos\alpha = q_A E - (av + bv^2)\cos\alpha \tag{2}$$

where v was the velocity of the jet, a and b were constants to be further determined theoretically or experimentally, q_A was the signed magnitude of the point A charge which was determined by the nature of the spinning solution, and E was the electric field intensity which was calculated using the applied voltage and the working distance.

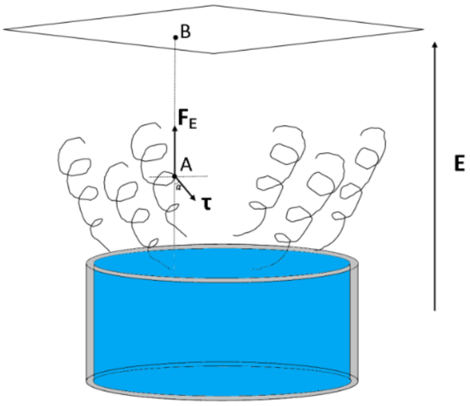

Figure 6. The forces at the point *A* of the jet in a FSE process.

According to above equations and figures, it could be found that the distribution of the electric field intensity played a very important role in a FSE process due to the multiple jets on the entire spinning area. To obtain a more effective electric field distribution under the same applied voltage, the solution reservoir of the FSE apparatus was modified, then MBE, MFSE, OSFSE and SSFSE devices were presented. It was necessary to simulate the distribution of the electric field intensity in these FSE processes for illustrating and comparing the spinning effects of them.

2.4 Simulation of electric field

The electric field distributions from the solution reservoir to the collector, which were produced in the different four self-made FSE processes, were simulated by Maxwell 3D. The electric field simulations for these FSE configurations were carried out using the following experimentally realized parameters: the copper reservoirs as positive pole were all a cylinder with a diameter of 40 mm and a height of 30 mm, the bulk conductivity of copper was 5.8 × 10^{11} us/cm, the electric conductivity of the polymer nozzles in the MBE was 0 us/cm, the electric conductivity of the PAN-DMF solution with a concentration of 10 wt% PAN and 1wt% SDBS was 2372 us/cm, the working distance was 180 mm, and the applied voltage was 40 kV.

2.5 Characterization

The morphology of PAN nanofibers were characterized by a scanning electron microscopy (Hitachi S4800, Hitachi, Tokyo, Japan). And the matrix morphology and fibrous diameter characterization were carried out by using Image J software (National Institute of Mental Health, Bethesda, MD, USA) upon 50 SEM images and 100 nanofibers at random in each SEM image. And the masses of PAN NFMs produced by four self-made FSEs devices were measured respectively by precise electronic balance (XJ120A, Precisa, Shanghai, China).

3. Result and discussion

3.1 Modeling electric field

The electric field simulation results of the different four solution reservoirs, which named MBE, MFSE, OSFSE and SSFSE device respectively, were obtained by Maxwell 3D, as illustrated in Fig. 7. Fig. 7 (A-1, B-1, C-1, D-1) showed the scalar plots of two-dimensional center section of the 3D electric field simulations respectively with the magnified view of the reservoir top edge, and the associated color legends were exhibited on the according left side where the colors illustrated the magnitude of the electric field. It could be found that when a voltage of 40 kV was applied to the devices, the electric field maximum appeared at the top edge of the reservoir. Fig. 7 (A-3, B-3, C-3, D-3) indicated the vector plots of the according simulations for illustrating electric field directions in the same region, where the arrow color showed the magnitude of the electric field. The vector plots depicted that the electric field directions where the jets formed at the solution surface of the reservoir were oriented directly towards the collector, which could be explained by the cylindrical symmetry of the reservoir and the cancellation of the vertical field components. And the electric field directions of the MBE device were relatively disordered, but those of the SSFSE device were the most orderly. Fig. 7 (A-2, B-2, C-2, D-2) and (A-4, B-4, C-4, D-4) respectively displayed the distributions of axial (0-180mm) and radial (0-100mm) electric field based on the center of the upper surface of the reservoir, which more clearly demonstrated the maximum electric field intensity values and their positions. The axial distribution curves showed the electric field intensities decreased with the increase of the distance from the solution surface. Moreover, according to the radial distribution curves, it was not difficult to find that all the electric field intensities dropped sharply near the top edge of the reservoir, which was caused by the electron transition from the copper to the air. And compared with the radial distribution curves of other FSEs devices, the electric field intensities of MBE device firstly decreased near the zero point then increased due to the influence of the polymer nozzle.

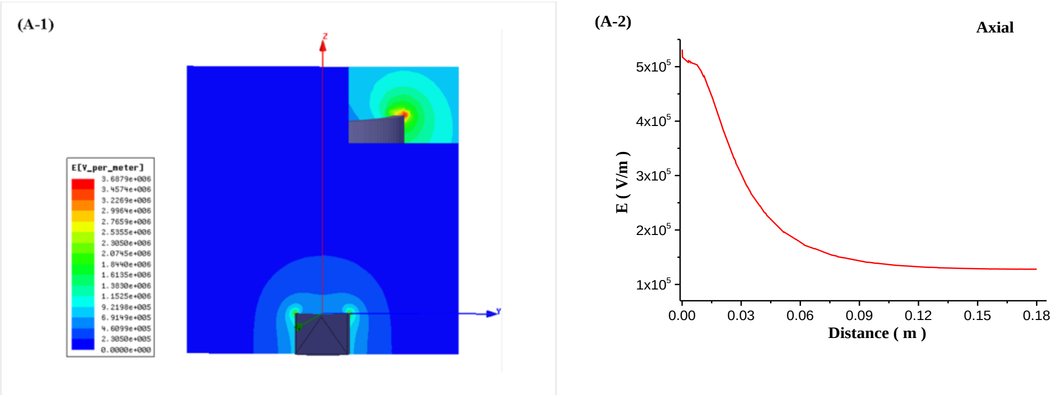

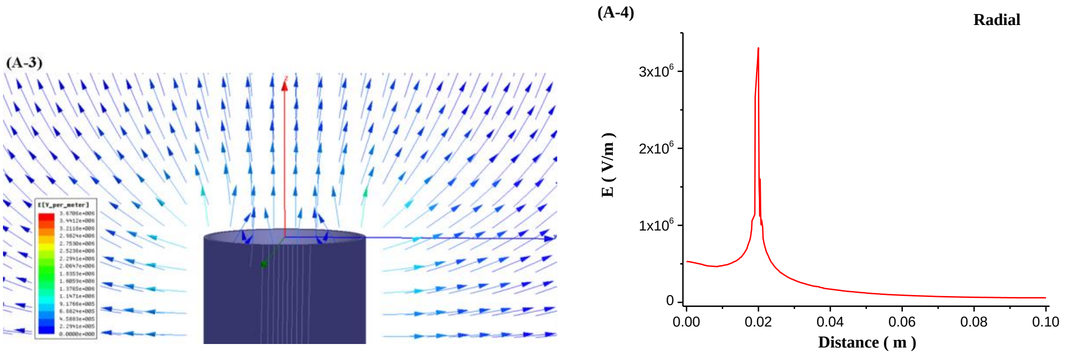

(A) MBE device

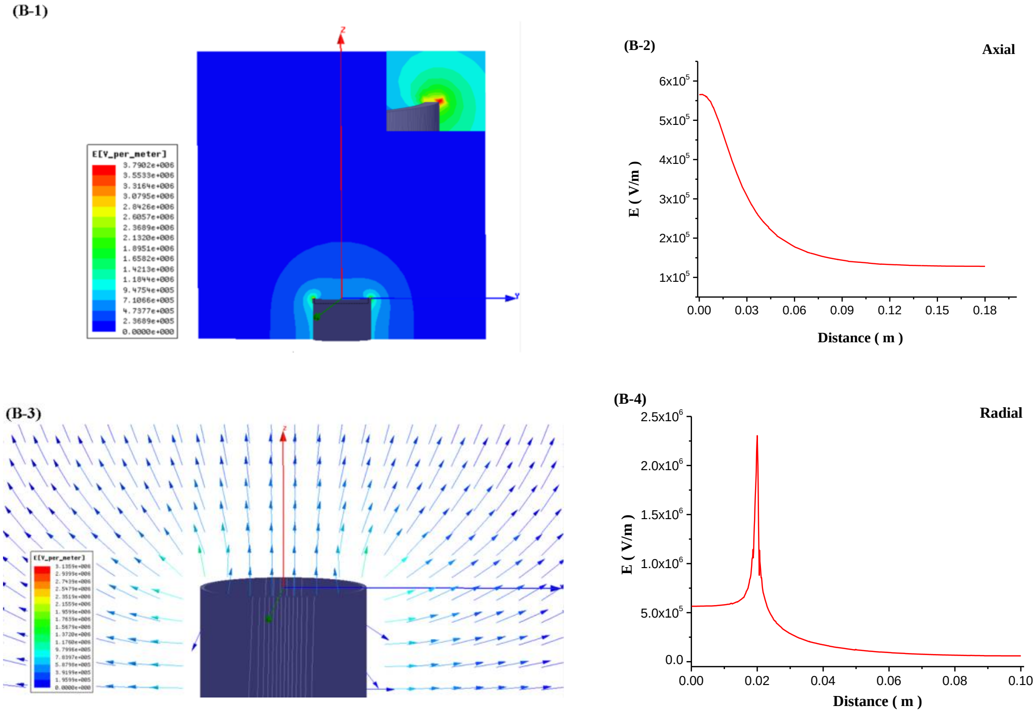

(B) MFSE device

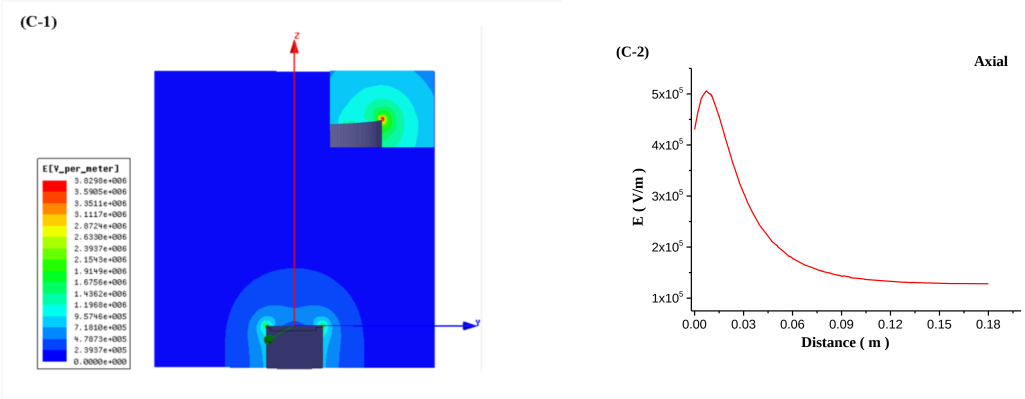

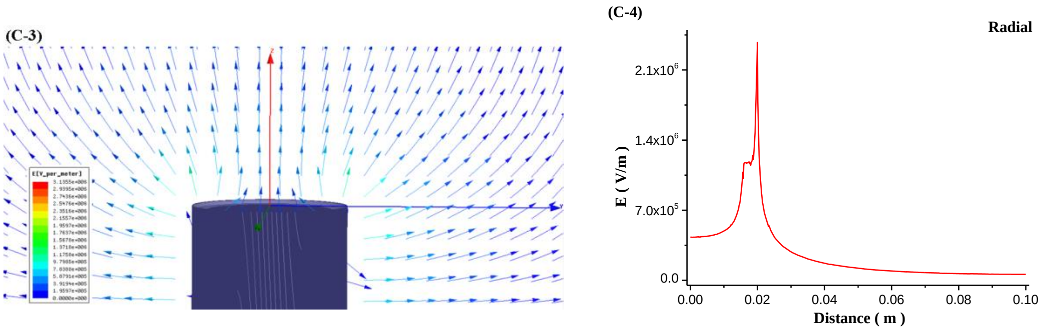

(C) OSFSE device

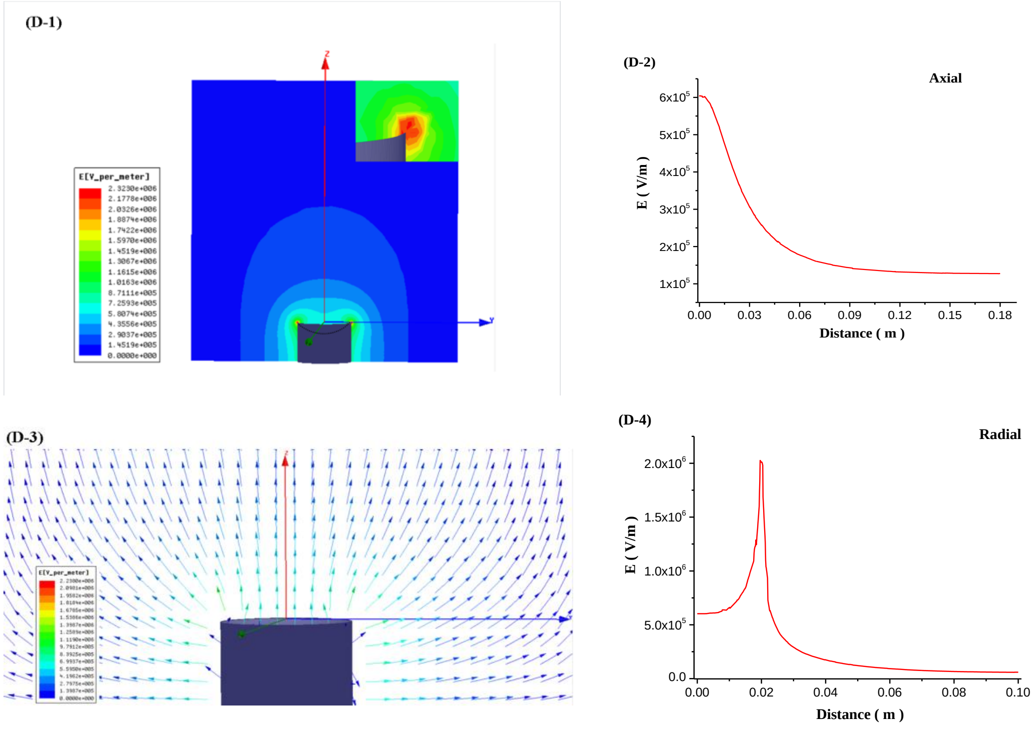

(D) SSFSE device

Figure 7. Simulation of the electric field distributions of MBE, MFSE, OSFSE and SSFSE device.

To further compare the uniformity of the electric fields of MBE, MFSE, OSFSE and SSFSE device, a parameter f was introduced as follows:

$$f = \frac{E_{\text{max}}}{E_{\text{av}}} \qquad (3)$$

where E_{max} was the maximum electric field intensity and E_{av} was the average electric field intensity.

Fig.8 showed the distribution charts of axial (0-180mm) electric field distribution through the center axis from the solution surface to the collector in four self-made FSE processes, and the calculated values of E_{max}, E_{av} and f were displayed in Table 2. There was little difference between the f-value of the axial direction in the four FSE processes. It illustrated the axial electric field distributions in the four FSE processes were similar,and the values of electric field intensity produced in the SSFSE device were the largest relatively.

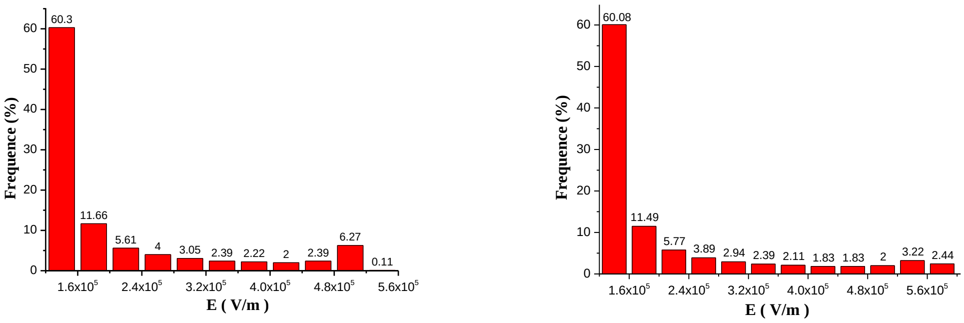

MBE device MFSE device

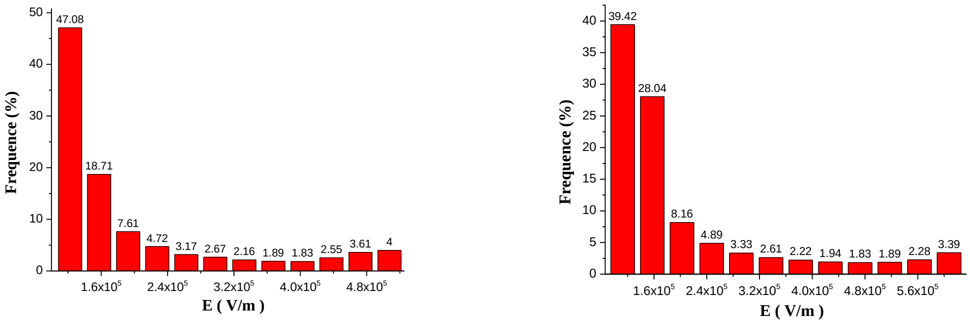

OSFSE device SSFSE device

Figure 5. Distribution chart of the electric field intensities on the center axial (0-180mm) directions in four self-made FSE processes.

Table 2. The calculated values of $E_{\max}$, E_{av} and f on the center axial (0-180mm) directions in four self-made FSE processes.

FES process	$E_{\max}$ (V/m)	E_{av} (V/m)	f
MBE	5.31×10^5	2.02×10^5	2.62
MFSE	5.66×10^5	2.07×10^5	2.75
OSFSE	5.06×10^5	2.02×10^5	2.52
SSFSE	6.04×10^5	2.08×10^5	2.88

Fig.9 showed the distribution charts of radial (0-20mm) electric field distribution from the center of the solution surface to the top edge of the reservoir in four self-made FSE processes, and the calculated values of $E_{\max}$, E_{av} and f were displayed in Table 3. It could be seen from Fig.9 that the abscissa values were obviously different. That meant the radial electric field distributions in the four FSE processes were quite different. To compare their difference clearly, detailed distributions of electric field intensity (E_R) on the radial (0-20mm) directions in four self-made FSE processes were illustrated as Table 3.

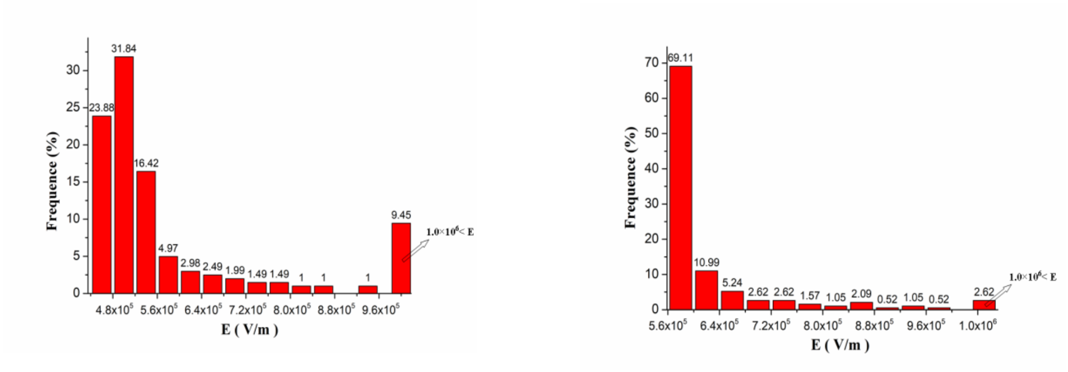

MBE device MFSE device

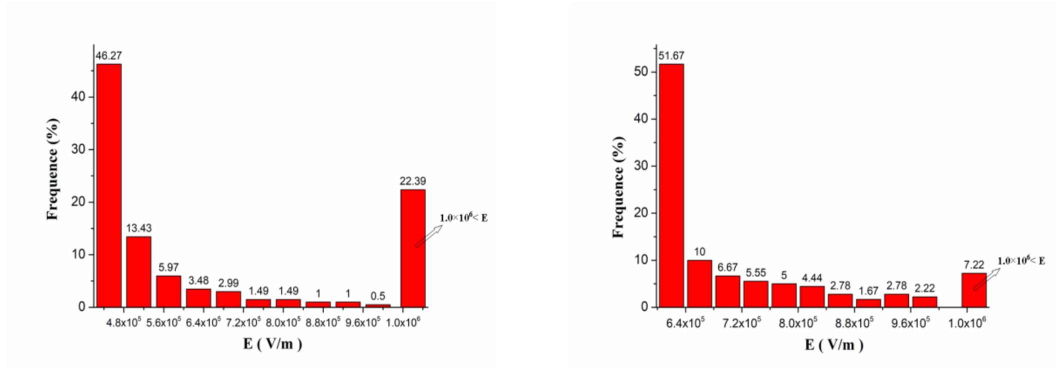

OSFSE device SSFSE device

Figure 9. Distribution chart of the electric field intensities on the radial (0-20mm) directions in four self-made FSE processes.

Table 3. Detailed distributions of the electric field intensities on the radial (0-20mm) directions in four self-made FSE processes.

E_R (V/m)	**Frequence (%)**			
	MBE	**MFSE**	**OSFSE**	**SSFSE**
$4.0\times10^5 < E_R \leq 4.4\times10^5$	0.00	0.00	24.88	0.00
$4.4\times10^5 < E_R \leq 4.8\times10^5$	0.00	0.00	21.39	0.00
$4.8\times10^5 < E_R \leq 5.2\times10^5$	23.88	0.00	9.95	0.00
$5.2\times10^5 < E_R \leq 5.6\times10^5$	31.84	0.00	5.97	0.00
$5.6\times10^5 < E_R \leq 6.0\times10^5$	16.42	69.11	3.48	0.00
$6.0\times10^5 < E_R \leq 6.4\times10^5$	4.98	10.99	2.49	51.67
$6.4\times10^5 < E_R \leq 6.8\times10^5$	2.99	5.24	1.99	10.00
$6.8\times10^5 < E_R \leq 7.2\times10^5$	2.49	2.62	1.99	6.67
$7.2\times10^5 < E_R \leq 7.6\times10^5$	1.99	2.62	1.00	5.55
$7.6\times10^5 < E_R \leq 8.0\times10^5$	1.49	1.57	1.00	5.00
$8.0\times10^5 < E_R \leq 8.4\times10^5$	1.49	1.05	1.00	4.44
$8.4\times10^5 < E_R \leq 8.8\times10^5$	1.00	2.09	0.50	2.78
$8.8\times10^5 < E_R \leq 9.2\times10^5$	1.00	0.52	1.00	1.67
$9.2\times10^5 < E_R \leq 9.6\times10^5$	0.00	1.05	0.50	2.78
$9.6\times10^5 < E_R \leq 1.0\times10^6$	1.00	0.52	0.50	2.22
$1.0\times10^6 < E_R$	9.50	2.62	22.39	7.22

E_{max}	3.31×10^6	1.14×10^6	2.38×10^6	2.03×10^6
E_{av}	6.82×10^5	6.20×10^5	6.90×10^5	8.00×10^5
f	4.84	1.77	3.48	2.50

From Fig.9 and Table 3, it could be found that the f-value of the MBE device was the largest, and the f-value of the MFSE device was the smallest. That meant the electric field distribution of the MBE device was the most non-uniform due to the influence of the polymer nozzle, which caused the multiple jets generated mainly on the top of the bubble produced by the nozzle and near the top edge of the copper reservoir, as shown in Fig.3(a). And the electric field distribution of the MFSE device without the tip discharge phenomena was the most uniform, but the values of the electric field intensities were the smallest, which resulted in the multiple jets produced primarily near the top edge of the reservoir, as illustrated in Fig.3(b). Moreover, there were some sides and corners at the reservoir edge of the OSFSE device (see Fig.2 (C and c)), which led to the non-uniform electric field distribution, the bigger electric field intensity and the multiple jets generated on the entire solution surface, as exhibited in Fig.3(c). Compared with the electric field distributions of other FSEs device, the f-value of the SSFSE device was relatively small, and its electric field intensities were the biggest, which caused the multiple jets produced on the entire solution surface, as displayed in Fig.3(d). This might be because the smooth spherical section of the reservoir made the electric field distribution more uniform, and the tip discharge phenomena appeared on the arc edge of the reservoir (see Fig.2 (D and d)) made the electric field intensity maximum. Therefore, comparing the electric field distributions of MBE, MFSE, OSFSE and SSFSE device, the results showed the electric field simulations could be used to explain the FSE processes observed by the high-speed camera, and the SSFSE device was the optimal FSE device due to the ordered electric field direction, the uniform electric field distribution and the largest electric field intensity, which would result in the high quality and yield of nanofibers obtained.

3.2 *Morphology of fibers*

The effects of four self-made FSE devices on the morphology of PAN nanofibers were investigated respectively by SEM. Fig.10 showed the SEM pictures and the according diameter distributions of PAN nanofibers prepared using the different FSE devices. And the relationship between the applied FSE devices and the average diameters of nanofibers fabricated was indicated in Fig.11, and the confidence intervals obtained were presented in Table 4. The standard deviations were high due to measuring nanofiber diameters by observing sample data. Therefore, a confidence interval was an estimated range of values which could include unknown diameters of nanofibers. The estimated range was calculated from a given set of sample data [24].

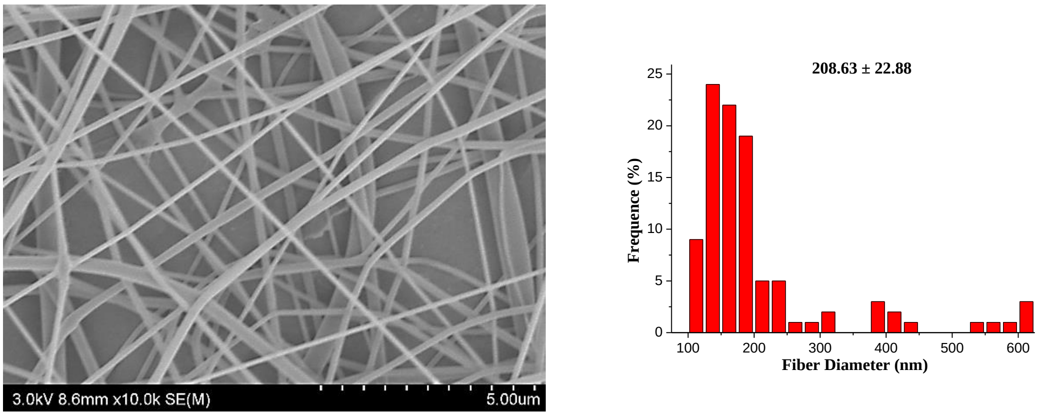

MBE device

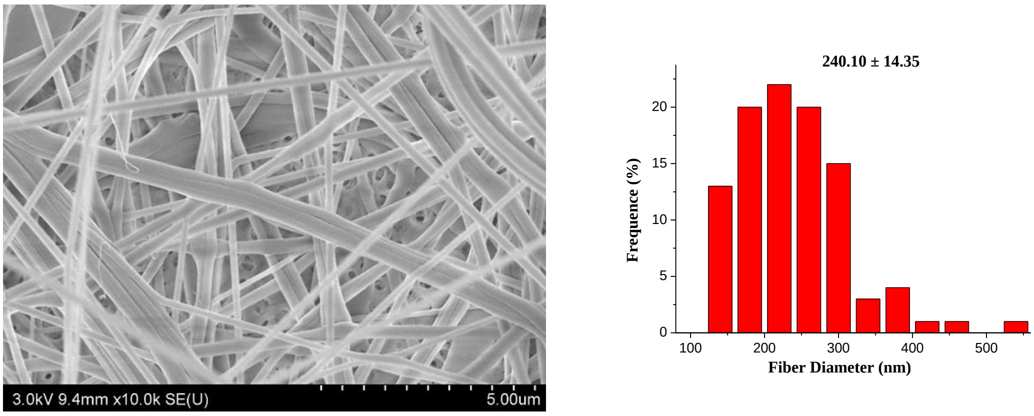

MFSE device

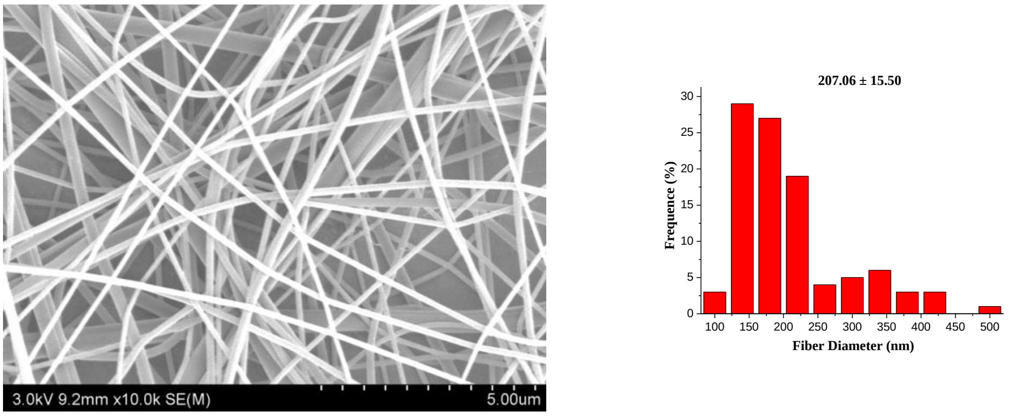

OSFSE device

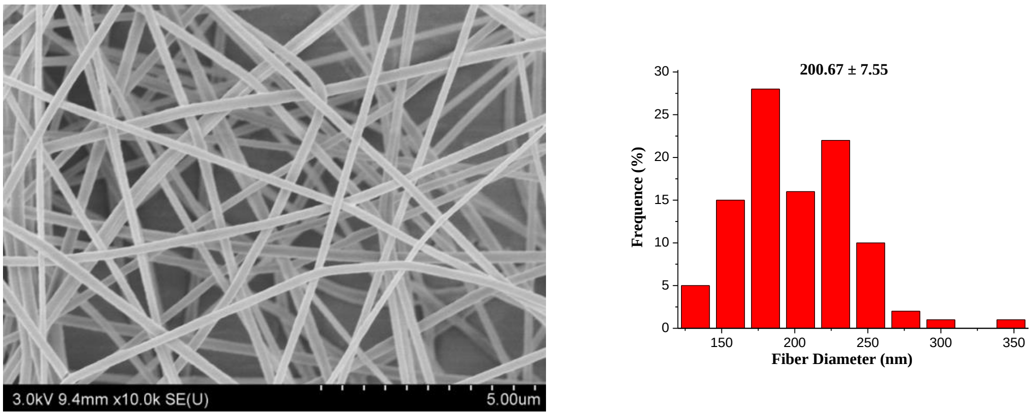

SSFSE device

Figure 10. SEM pictures and the according diameter distribution of the PAN nanofibers obtained by four self-made FSE devices.

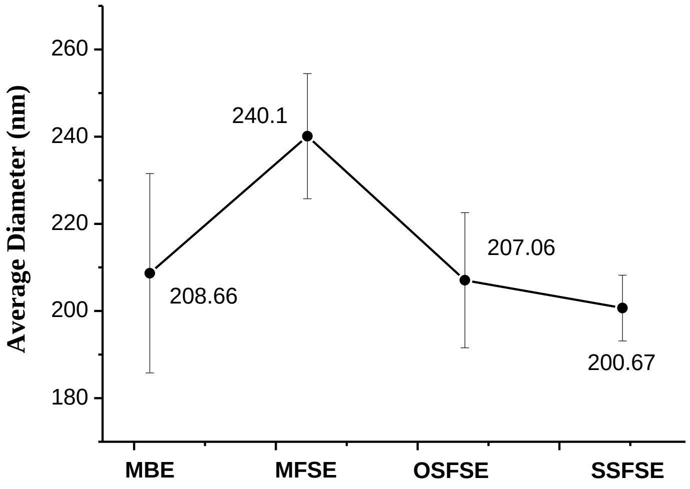

Figure 11. Average diameter of PAN nanofibers.

The results from Figs. 10 and 11 showed the average diameter of nanofibers prepared by MFSE device was the biggest than other self-made FSEs device, and the average diameters of nanofibers obtained by MBE, OSFSE, and SSFSE device were similar to each other. However, it could be seen from Table 4 that the nanofiber distributions of MFSE and SSFSE device demonstrated more uniformity because of their relatively smaller confidence intervals. The diameter variation trend of the nanofibers fabricated using the four FSEs devices could be explained by the previous electric field simulation results, as shown in Fig.7 and Table 3. In Fig.7 and Table 3, the electric field intensity of MFSE device was the smallest. According to Eq. (2), the larger the electric field intensity was, the larger the electric field force would be, which made the jet more stretched and the nanofiber diameter become smaller. Therefore, the diameter of nanofibers prepared by MFSE device was the biggest due to the smallest electric field intensity. In addition, the smaller the f-value of the FES device, the more uniform the electric field distribution, resulting in the more uniform diameter distribution of the nanofibers. As a result, the distributions of the nanofibers by MFSE and SSFSE device were more uniform because of their smaller f-value, which meant the uniform electric field distributions. The quality of the nanofibers prepared by MBE, MFSE, OSFSE and SSFSE device was compared to each other, and it could be found that the quality of nanofibers obtained by the SSFSE device was highest, which was consistent with the electric field simulation results.

Table 4. Effects of four different FSEs devices on the nanofiber diameters.

FES device	Average diameter (nm)	Standard deviation (nm)	Confidence interval (nm)
MBE	208.66	116.72	22.88
MFSE	240.06	73.21	14.35
OSFSE	207.06	79.08	15.5

SSFSE	200.67	38.52	7.55

3.3 Yield of PAN nanofibers

Fig.12 illustrated the yields of PAN nanofibers fabricated by the different FSE devices. It could be seen that the yield of MBE device was 4.37 g/h. In our previous work [23], this device was used to prepare silk fibroin (SF) nanofibers with a yield of 3.1 g/h, but the applied voltage was 60 kV. This was because PAN has better spinnability than SF. When the structure of the reservoir was modified, the electric field distribution in the FSE process changed, and the yields of nanofibers varied using the same voltage, distance and spinning solutions. As shown in Fig.12, the yield of SSFSE was the highest, followed by OSFSE, MFSE and MBE device. This might be because that the generated bubbles wasted energy which could make the charged jets move faster during the MBE process, and as a result the yield of PAN nanofibers was lower. As for MFSE, OSFSE, and SSFSE device, the yields varied with the change of the electric field intensities. According to the distribution of the electric field intensities in the FES processes as displayed in Fig.7 and Table 3, the yield of nanofibers prepared by the SSFSE device was highest, which was in agreement with the experimental results.

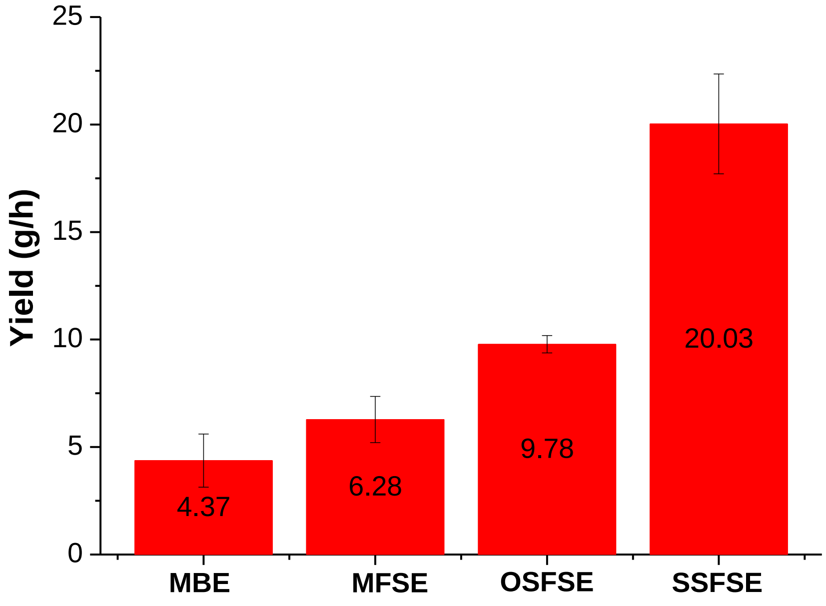

Figure 12. Yield of the PAN nanofibers via different setups.

4. Conclusion

In this paper, four different self-made FSE devices, MBE, MFSE, OSFSE and SSFSE device, were presented to obtain high quality PAN nanofibers in large quantity. Through the using of Maxwell 3D, the preparation mechanisms of four kinds of FSE devices were studied by the simulations of the electric field distribution, due to the importance of electric field in the FSE process. The simulation results showed the electric field distribution of the MBE device was the most non-uniform, and the electric field intensities of the MFSE device were the smallest. Comparing the electric field distributions of these four FSEs devices, the SSFSE device was the optimal FSE device due to the ordered electric field direction, the uniform electric field distribution and the largest electric field intensity.

Then the effects of these four FSE devices on the morphology and yield of nanofibers were investigated experimentally. It could be seen that the average diameter of nanofibers prepared by MFSE device was the biggest, and the nanofiber distributions of MBE device was the most non-uniform. Moreover, the nanofiber distributions of MFSE and SSFSE device demonstrated more uniformity. The experimental data were in accordance with the simulation and theoretical analysis results. The results showed the SSFSE device was the optimal FSE device because of the highest quality and yield of nanofibers, and its yield could reach 20.03 g/h at the applied voltage of 40 kV.

Author Contributions

L. X. and Y. F. designed the experiments. Y. F. performed the experiments and the characterization, analyzed the data and wrote the paper. L. X. supervised data analysis and revised the paper.

Funding

This research was funded by National Natural Science Foundation of China: No. 11672198, the National Key R&D Program of China: 2017YFC1103602, Six Talent Peaks Project of Jiangsu Province: GDZB-050, and the Foundation project of Jiangsu Advanced Textile Engineering Technology Center (Grant No. XJFZ/2018/15).

Acknowledgments

The work is supported financially by National Natural Science Foundation of China (Grant No. 11672198), Six Talent Peaks Project of Jiangsu Province (Grant No.GDZB-050), the National Key R&D Program of China: 2017YFC1103602, Foundation project of Jiangsu Advanced Textile Engineering Technology Center (Grant No. XJFZ/2018/15), and PAPD (A Project Funded by the Priority Academic Program Development of Jiangsu Higher Education Institutions).

Abbreviations

Free surface electrospinning (FSE); Modified bubble-electorspinning (MBE); Modified free surface electorspinning (MFSE); Oblique section free surface electorspinning (OSFSE); Spherical section free surface electrospinning (SSFSE); electrospinning (ES)； Polyvinylpyrrolidone (PVP); Polyacrylonitrile (PAN); Polyvinyl alcohol (PVA); Poly(ethylene oxide) (PEO); Silk fibroin (SF); Sodium dodecyl benzene sulfonate (SDBS); N,N-dimethylformamide (DMF)

Availability of Data and Materials

All data generated or analyzed during this study were included within the article.

References

[1] F. Mehrpouya, J. Foroughi, S. Naficy, J. M. Razal and M. Naebe, Nanostructured electrospun hybrid graphene/polyacrylonitrile yarns. *Nanomaterials*, 2017, **7(10),** 293. DOI: 10.3390/nano7100293

[2] T. Macdonald, J. Xu, S. Elmas, Y. Mange, W. Skinner, H. Xu and T. Nann, Nio nanofibers as a candidate for a nanophotocathode. *Nanomaterials,* 2014, **4(2),** 256-266. DOI: 10.3390/nano4020256

[3] M. Khandaker, S. Riahinezhad, H. G. Jamadagni, T. L. Morris, A. V. Coles and M. B. Vaughan, Use of polycaprolactone electrospun nanofibers as a coating for poly(methyl methacrylate) bone cement. *Nanomaterials,* 2017, **7(7),** 175. DOI: 10.3390/nano7070175

[4] T. C. M. Julien, M. D. Subramanyam, H. C. Katakam, S. Lee, S. Thomas and J. P. Harmon, Ultrasoft polycarbonate polyurethane nanofibers made by electrospinning: fabrication and characterization. *Polym. Eng. Sci.,* 2019. DOI: 10.1002/pen.25021

[5] M. Wortmann, N. Frese, L. Sabantina, R. Petkau, F. Kinzel and A. Gölzhäuser, New polymers for needleless electrospinning from low-toxic solvents. *Nanomaterials (Basel, Switzerland),* 2019, **9(1),** 52. DOI: 10.3390/Nano 9010052

[6] M. Eslamian, M. Khorrami, N. Yi, S. Majd and M. R. Abidian, Electrospinning of highly aligned fibers for drug delivery applications. *J. Mater. Chem. B.,* 2019, **7(2).** DOI: 10.1039/C8TB01258J

[7] W. Zhao, S. Ci, X. Hu, J. Chen and Z. Wen, Highly dispersed ultrasmall nis nanoparticles in porous carbon nanofiber anodes for sodium ion batteries. *Nanoscale,* 2019, **11(11)**. DOI: 10.1039/C9NR00160C

[8] O. O. Dosunmu, G. G. Chase, W. Kataphinan and D. H. Reneker, Electrospinning of polymer nanofibres from multiple jets on a porous tubular surface. *Nanotechnology,* 2006, **17(4),** 1123. DOI: 10.1088/0957-4484/17/4/046

[9] J. S. Varabhas, G. G. Chase and D. H. Reneker, Electrospun nanofibers from a porous hollow tube. *Polymer,* 2008, **49(19),** 4226-4229. DOI: 10.1016/j.polymer.2008.07.043

[10] B. Ding, E. Kimura, T. Sato, S. Fujita and S. Shiratori, Fabrication of blend biodegradable nanofibrous nanwoven mats via multi-jet electrospinning. *Polymer,* 2004, **45(6),** 1895-1902. DOI： 10.1016/j.polymer.2004.01.026

[11] T. Krishnamoorthy, M. Z. Tang, A. Verma, A. S. Nair, D. Pliszka, S. G. Mhaisalkar and S. Ramakrishna, A Facile Route to Vertically Aligned Electrospun SnO2 Nanowires on a Transparent Conducting Oxide Substrate for Dye-Sensitized Solar Cells. *J. Mater. Chem.,* 2012, **22(5),** 2166–2172. DOI:10.1039/C1JM15047B

[12] I. G. Kim, J. H. Lee, A. R. Unnithan, C. H. Park and C. S. Kim, A Comprehensive Electric Field Analysis of Cylinder-Type Multi-Nozzle Electrospinning System for Mass Production of Nanofibers. *J. Ind. Eng. Chem.,* 2015, **31,** 251–256. DOI:10.1016/j.jiec.2015.06.033.

[13] H. Niu, X. Wang and T. Lin, Upward needleless electrospinning of nanofibers. *J. Eng. Fibers Fabr.,* 2012, **7(3),** 17-22. DOI: 10.1177/155892501200702s03

[14] J. H. He, Y. Liu, L. Xu, J. Y. Yu and G. Sun, BioMimic fabrication of electrospun nanofibers with high-throughput. *Chaos, Solitons Fractals,* 2008, **37(3),** 643-651. DOI: 10.1016/j.chaos.2007.11.028

[15] R. X. Chen, Y. Q. Wan, N. Si, J. H. He, F. Ko and S. Q. Wang, Bubble rupture in bubble electrospinning. *Thermal Science,* 2015, **19(4),** 1141-1149. DOI: 10.2298/TSCI1504141C

[16] N. M. Thoppey, J. R. Bochinski, L. I. Clarke and R. E. Gorga, Edge electrospinning for high throughput production of quality nanofibers. *Nanotechnology,* 2011, **22,** 345301 (11pp). DOI: 10.1088/0957-4484/22/34/345301

[17] G. Jiang and X. Qin, An improved free surface electrospinning for high throughput manufacturing of core–shell nanofibers. *Mater. Lett.,* 2014, **128,** 259-262. DOI: org/10.1016/j.matlet.2014.04.074

[18] D. Wu, X. Huang, X. Lai, D. Sun and L. Lin, High throughput tip-less electrospinning via a circular cylindrical electrode. *J. Nanosci. Nanotechnol.*, 2010, **10(7),** 4221-4226. DOI: org/10.1166/jnn.2010.2194

[19] H. U. Shin, Y. Li, A. Paynter, K. Nartetamrongsutt and G. G. Chase, Microscopy analysis and production rate data for needleless vertical rods electrospinning parameters. *Data in Brief,* 2015, **5,** 41-44. DOI: 10.1016/j.dib.2015.08.005

[20] S. Moon, M. Gil and K. J. Lee, Syringeless electrospinning toward versatile fabrication of nanofiber web. *Sci. Rep.*, 2017, **7,** 41424. DOI: 10.1038/srep41424

[21] Z. Shao, L. Yu, L. Xu and M. Wang, High-throughput fabrication of quality nanofibers using a modified free surface electrospinning. *Nanoscale. Res. Lett.*, 2017, **12(1),** 470. DOI: 10.1186/s11671-017-2240-4

[22] L. Yu, Z. B. Shao, L. Xu and M. D. Wang, High throughput preparation of aligned nanofibers using an improved bubble-electrospinning. *Polymers*, 2017, **9**, 658. DOI: 10.3390/polym9120658

[23] F. Yue, X. Lan and W. Mingdi, High-throughput preparation of silk fibroin nanofibers by modified bubble-electrospinning.*Nanomaterials,* 2018, **8(7),** 471-. DOI: 10.3390/nano8070471

[24] Z.Y. Sun, C.X. Fan, X.P. Tang, J.H. Zhao, Y.H. Song, Z.B. Shao and L. Xu, Characterization and antibacterial properties of porous fiberscontaining silver ions. *Appl. Surf. Sci.,* 2016, **387,** 828–838. DOI: 10.1016/j.apsusc.2016.07.015

Graphica Abstract